Molecular Simulation of Disjoining-Pressure Isotherms for Free Aqueous Thin Films

Divesh Bhatt, John Newman, and C. J. Radke*

Department of Chemical Engineering, University of California, Berkeley, California 94720-1462

Received: March 31, 2003; In Final Form: September 15, 2003

We present canonical-ensemble molecular-dynamics (MD) simulations of disjoining-pressure isotherms for symmetric, free aqueous thin films. For such symmetric films, the disjoining pressure is purely attractive. Lifshitz's theory, based on continuum dispersion forces, predicts that the disjoining pressure varies as an inverse cube of film thickness, with a constant of proportionality that can be calculated within the framework of this theory. Our MD results indicate that Lifshitz theory, which assumes a slab geometry for the water density profile and neglects the fluid structure, underpredicts the disjoining pressure by about 50 times for films ranging from about 1 to 2 nm at 479 K. To investigate more closely actual experimental conditions, we also perform simulations of water films surrounded by inert gas molecules. The additional gas component adds an extra thermodynamic degree of freedom to the system, allowing for the chemical potential of the water in the external liquid reservoir to be maintained constant, thus mimicking actual experimental conditions more closely. Inclusion of inert gas at high pressure leads to a disjoining-pressure isotherm that is about twice as large as that without the inert gas for pressures in the liquid reservoir about 2 orders of magnitude larger than the vapor pressure of water at 479 K. Finally, we qualitatively show that upon decreasing the added inert-gas pressure, we obtain a different set of thin films with a smaller magnitude of the disjoining pressures.

Introduction

A thin liquid film of a few tens of nanometers in thickness and bounded on both sides by gas or vapor (and hence, a free liquid thin film) is of importance in systems such as foams where typical aqueous surfactant-stabilized films are surrounded by air. In thin liquid films, the normal component of pressure is constant across the interface, whereas the tangential component varies as a function of position perpendicular to the liquid/vapor interface.[1−3] However, the constant normal pressure in the film region is not the same as the isotropic pressure in the bulk liquid with which the film is in contact; the difference between these two pressures is the disjoining pressure, Π.[2,3] When reported as a function of film thickness, h, at constant temperature, $\Pi(h)$ is called the disjoining-pressure isotherm. Foam (and emulsion) stability is, in large part, determined by the disjoining-pressure isotherm.[4,5]

Numerous experimental studies are available for the disjoining-pressure isotherms of aqueous thin films containing surfactants,[6−13] and a few for aqueous films stabilized with proteins[14,15] and polyelectrolytes.[16] Likewise, there are systematic molecular simulations in the literature[17−24] of the forces in confined thin films (i.e., confined between solid walls) where oscillatory forces can arise at small separation. However, molecular simulations of the forces in free thin liquid films are almost nonexistent.[25] Long wavelength fluctuations (i.e., due to thermal capillary waves) in systems with free interfaces tend to destabilize these metastable films.[26,27] Moreover, in the absence of a bounding surface, the liquid can evaporate (or the vapor can condense), making it difficult to maintain a liquid film during the course of a simulation.

The classical thin-film theory of van der Waals forces, the Hamaker theory,[28] and also the later, more detailed theory of Lifshitz[29] indicate that the disjoining pressure varies as the inverse cube of film thickness. However, in these theories, a slab model of the density profile is invoked, and the liquid structure is ignored. In our previous simulation work with Lennard-Jones (LJ) thin films,[25] we found that the available theories of thin-film forces drastically underpredict the disjoining pressure. With the aid of a density-functional theory, we relaxed some of the assumptions of the above theories and found a profound effect of the density profile and the fluid structure on the disjoining-pressure isotherm that brings theory and simulation closer into agreement.

Here we extend our previous work on LJ fluids to aqueous thin films. In particular, we perform molecular-dynamics (MD) simulations of free thin liquid films to calculate the disjoining-pressure isotherm in a liquid/vapor system. Accordingly, we investigate the attractive component to the overall disjoining pressure due to water, and we address the question of how thin a free film must be before deviations from continuum Lifshitz theory might emerge. Since a one-component system does not allow the properties of the reservoir (pressure or the chemical potential) to be maintained constant for films of different thicknesses, we additionally simulate a water film in the presence of inert gas. The additional gas component increases the thermodynamic degrees of freedom by one, allowing the reservoir to be maintained at a constant water chemical potential or at a constant pressure for films of different thicknesses. In both of these systems (one- and two-components), the films are purely attractive. Thus, they are unstable to long-wavelength fluctuations[26] and cannot be studied in real experiments. Fortunately, in computer simulation, the finite box size limits

* To whom correspondence should be addressed. Phone 510-642-5204. Fax 510-642-4778. E-mail radke@cchem.berkeley.edu.

10.1021/jp030415h CCC: $25.00
Published on Web 11/04/2003

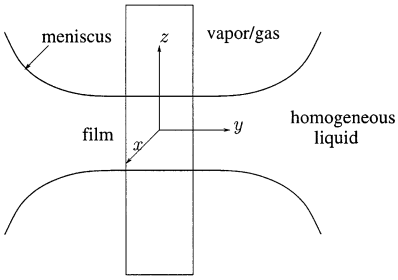

Figure 1. A schematic of the thin-film system. The film is in equilibrium with the bulk liquid connected to it via the Plateau-border meniscus (which is not included in the simulation). A vapor region surrounds the film on both sides.

the long-wavelength fluctuations. Nevertheless, evaporation/condensation processes remain a challenge to maintaining the film.

One-Component Water Films

Simulation Details. The intermolecular potential model we choose for simulating water is the extended simple-point-charge (SPC/E) model of Berendsen et al.[30] In this model, the potential energy between two water molecules i and j is

$$u_{ij} = 4\epsilon_{oo}\left[\left(\frac{\sigma_{oo}}{r_{io,jo}}\right)^{12} - \left(\frac{\sigma_{oo}}{r_{io,jo}}\right)^{6}\right] + \frac{1}{4\pi\epsilon_0}\sum_{a=1}^{3}\sum_{b=1}^{3}\frac{q_{ia}q_{jb}}{r_{ia,jb}} \quad (1)$$

where ϵ_{oo} and σ_{oo} are, respectively, the Lennard-Jones (LJ) energy and size parameters for the oxygen atoms in each water molecule, $r_{ia,jb}$ is the distance between atom a ($a = 1$ and 3 for hydrogen atoms, and $a = 2$ for oxygen) of molecule i and atom b of molecule j, ϵ_0 is the permittivity of free space, and q_{ia} is the (partial) charge on atom a of molecule i. In the SPC/E model, $\epsilon_{oo} = 650.2$ J/mol and $\sigma_{oo} = 0.3166$ nm. In addition, the partial charge on each oxygen site is $q_{io} = 0.8476e$, and on each hydrogen site it is $|q_{io}|/2$, where e is the charge of an electron.

A schematic of a two-dimensional projection of the thin-film system, for which the disjoining pressure is to be calculated, is shown in Figure 1. In the figure, a thin liquid film surrounded by vapor/gas is connected to a bulk liquid through the Plateau-border meniscus, which is not included in the simulation. Since for symmetric films with no surface active agents the disjoining pressure is negative, the curvature of the Plateau-border meniscus is actually opposite that shown. Figure 1 is drawn for the case of a stable thin film under the influence of a net repulsive disjoining force. The liquid/vapor interface is perpendicular to the z-direction. Also shown in the figure is the simulation box that symmetrically encompasses a portion of the flat part of the thin film. Periodic-boundary conditions are applied in all coordinate directions, and the minimum-image convention is adopted.

We simulate films with canonical-ensemble MD using the Nose−Hoover thermostat.[31−34] The number of water molecules is fixed at 534 even as we thin the films in subsequent simulations. Accordingly, the edge lengths of the simulation box parallel to the film interface (L_x and L_y) are varied. The smallest value of L_x ($=L_y$) (i.e., for the thickest film) is 2 nm, whereas L_z is kept constant at 10 nm. Alejandre et al.[35] have established that the thermodynamic properties, such as the coexistence densities and the surface tension, of systems of this size are independent of system size. More details on the edge lengths of the simulation boxes for each film are given later. Long-range coloumbic interactions are evaluated by using the Ewald summation method.[36,37] In addition, instead of adding tail corrections, we use an Ewald-like technique to calculate the LJ part of the interaction.[37,38] The details on how the parameters for the Ewald summation are calculated are given in Appendix A. All films are first equilibrated for about 100 ps with an integration time step of about 2.5 fs, followed by about 300 ps of production runs.

As mentioned in the Introduction, the disjoining pressure is defined as

$$\Pi = p_N - p_L \quad (2)$$

where p_N is the normal pressure in the film and p_L is the pressure in the homogeneous liquid at the same chemical potential as the film (i.e., p_L is the pressure in the homogeneous liquid reservoir constituting the constant-curvature part of the meniscus). From eq 2, it is apparent that both the normal pressure and the chemical potential are the quantities of interest in calculating the disjoining pressure. We calculate the normal pressure and chemical potential in the same manner as in our previous work.[25] Specifically, we bin our simulation box perpendicular to the interface and then evaluate the normal component of the Irving and Kirkwood (IK) pressure tensor.[35,39−41] Widom's particle insertion method is used for the chemical potential.[42] Both the normal component of the pressure tensor and the chemical potential are evaluated in the gas phase because of statistical uncertainties in the dense liquid phase.

Once p_N is calculated, we establish p_L at the same chemical potential as in the film. To accomplish this we follow our earlier work[25] and integrate the one-component Gibbs−Duhem equation at constant temperature from the saturation state to the condition in the liquid in the meniscus (that is in equilibrium with the film), assuming that the density of the liquid is constant between the two states of interest. The result is[25,43]

$$p_L - p_{sat,w} = \rho_{L,w}(\mu_w - \mu_{sat,w}) \quad (3)$$

where $p_{sat,w}$ is the vapor pressure of the liquid (water) in the saturation state, μ_w is the chemical potential of water in the thin film, and $\mu_{sat,w}$ is the saturation chemical potential of water all at the temperature of interest.

To obtain the isothermal saturation state, we simulate a thick film corresponding to the bulk liquid/vapor coexistence point. Thus, p_L at the chemical potential of the film is established from eq 3, and the disjoining pressure follows in a straightforward manner from eq 2. The thermodynamics of one-component systems is presented in greater detail elsewhere.[25]

Results. First, we simulated a thick film at 300 K. The coexistence liquid density at this temperature was obtained as 0.998 g/cm^3. Also, the surface tension was obtained from the expression[35]

$$\gamma = \frac{L_z}{2}\left\langle p_{zz} - \frac{1}{2}(p_{xx} + p_{yy})\right\rangle \quad (4)$$

where p_{ii} is the ii component of the pressure tensor. We obtained $\gamma = 69.5 \pm 3.3$ mN/m, which agrees well with both the experimental result and the previous simulations for SPC/E water that employed a tail correction for the LJ potential beyond the cutoff.[35,44] These results validate our simulation, and show that by treating the LJ part of the interaction by an Ewald-type

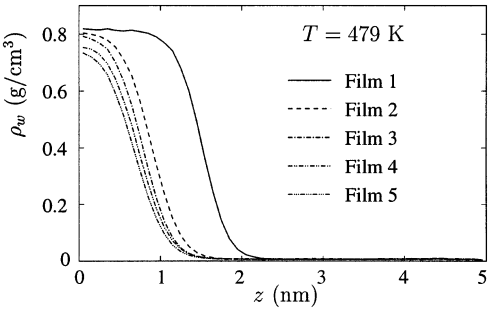

Figure 2. Density profiles for five different water films at 479 K. Film 1 is a thick film, and Films 2 to 5 are progressively thinner.

TABLE 1: Simulated Quantities of One-Component Water Films at 479 K[a]

Film	$L_x(=L_y)$ (nm)	$\rho_{v,w}$ (g/cm^3)	μ_w*	p_N (MPa)	Π (MPa)	h (nm)
1	2.53	0.0051	−33.1	0.70	0	3.01
2	3.27	0.0065	−32.7	0.92	−11.8	1.77
3	3.51	0.0066	−32.4	0.91	−20.6	1.52
4	3.65	0.0073	−31.9	1.13	−35.4	1.39
5	3.81	0.0075	−31.0	1.16	−61.8	1.26

[a] Film 1 depicts the bulk coexistence at this temperature.

summation we are considering the whole LJ interaction without the need for a tail correction. Unfortunately, the coexistence vapor density obtained at 300 K is negligibly small. Since our method relies on calculating the normal pressure and the chemical potential of the system in the low-density vapor region (the statistical uncertainty in the liquid phase is too large to allow a meaningful estimate), disjoining-pressure calculations at 300 K are precluded.

Hence, we chose a higher temperature. However, for temperatures too close to the critical point, it is practically impossible to maintain a film. Thus, we set $T = 479$ K as the simulation temperature. For a thick film at this temperature, we obtained a value of 0.817 g/cm^3 for the liquid coexistence density and a vapor density of 0.0051 g/cm^3. Additionally, the surface tension is 33.5 ± 3.1 mN/m. Again, these values agree well with previous simulation results for SPC/E water, as well as with experimental results.[35]

Figure 2 depicts the density profiles for five different films at 479 K. Film 1 is a thick film (as mentioned above) corresponding to zero disjoining pressure. Films 2−5 are progressively thinner films. Clearly, the densities at the centers of the thin films are less than the bulk coexistence density (corresponding to film 1). This result is similar to our previous result on LJ films. Table 1 lists the relevant simulation properties of the films. Column 2 shows L_x ($=L_y$) used for each film, column 3 depicts the vapor density (in g/cm^3), column 4 lists the nondimensional chemical potential of water (with respect to ϵ_{oo}) relative to the density-independent part,[45] and column 5 gives the film normal pressure (in MPa). As we see, the chemical potential increases as the film thickness decreases.

From eqs 2 and 3, we can calculate the disjoining pressures, as presented in column 6 of Table 1. In addition, the film thickness for each of these films is calculated by using a Gibbs-motivated idea that the film is a step function between the vapor and the liquid densities up to the dividing surface and that there is zero adsorption at the dividing surface. This is a convenient definition and has been used in the literature to define the film thickness.[46] The resulting film thickness is shown in column 7 of Table 1.

Hamaker theory suggests that $\Pi = -A_H/6\pi h^3$,[47] with the Hamaker constant A_H given in Lifshitz's theory for two half

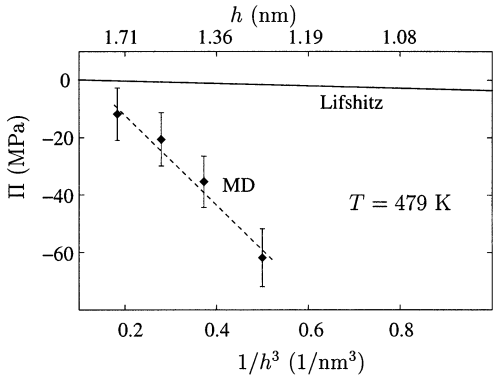

Figure 3. Disjoining-pressure isotherm for pure water films at 479 K. The prediction from Lifshitz's theory is shown as the solid line. Compared to MD results, the slope of the theoretical line is very small.

spaces of media 1 and 2 separated by another medium 3 of thickness h as[48,49]

$$A_H = -\frac{3}{2}kT\sum_{n=0}^{\infty}{}'\int_{r_n}^{\infty} x \ln\{[1-\Delta_{13}\Delta_{23}e^{-x}][1-\bar{\Delta}_{13}\bar{\Delta}_{23}e^{-x}]\}\,dx \tag{5}$$

where the prime indicates that the first term in the summation is multiplied by one-half and

$$\Delta_{jk} = \frac{\epsilon_j s_k - \epsilon_k s_j}{\epsilon_j s_k + \epsilon_k s_j}, \qquad \bar{\Delta}_{jk} = \frac{s_k - s_j}{s_k + s_j}$$

$$s_k^2 = x^2 + \left(\frac{2\zeta_n h}{c}\right)^2(\epsilon_k - \epsilon_3), \qquad r_n = \frac{2h\zeta_n\sqrt{\epsilon_3}}{c}$$

$$\zeta_n = \frac{2\pi nkT}{\hbar}, \qquad \epsilon_k = \epsilon_k(i\zeta_n) \tag{6}$$

where indices j and k refer to the types of media, c is the speed of light in a vacuum, k is the Boltzmann constant, $\hbar$ is Planck's constant divided by 2π, and ζ_n are the sampling frequencies of the dielectric function $\epsilon_k(i\zeta)$. For film thicknesses of interest (between 1 and 2 nm) A_H for water/air films is 5.7×10^{-20} J at 300 K. Upon using the approximate method suggested by Dagastine et al.[49] to estimate the Hamaker constant at different temperatures, $A_H \approx 6.2 \times 10^{-20}$ J at 479 K.

Figure 3 compares the result obtained from MD and Lifshitz's theory. Π is plotted here as a function of $1/h^3$ from both the MD (using the above definition of film thickness), shown with solid diamonds, and Lifshitz theory, shown with a solid line. h is labeled on the top abscissa in a nonlinear scale for reference. A straightline fit to our MD results is also shown as a dashed line, giving $A_H = 3 \times 10^{-18}$ J. Although the error bars in the disjoining-pressure values, established from the corresponding errors in the normal pressure and the chemical potential, are large (≈10 MPa), we can definitely say that Lifshitz's theory underpredicts the value of the disjoining pressures for the range of film thicknesses considered by about 50 times.

One explanation for the larger magnitude of the observed disjoining pressure is the so-called "hydrophobic force",[50] since the liquid water/vapor interface is sometimes considered as hydrophobic.[50] However, in our previous work on LJ fluids, we found a smaller (but still about an order of magnitude) difference between simulation and Hamaker theory.[25] There we

explained the larger magnitude of simulated disjoining pressure using a density-functional theory and concluded that the difference is due to the fact that Hamaker theory neglects the density profile and the fluid structure (i.e., that it neglects the granularity of the fluid). An identical argument seems applicable to water as well. Similar discrepancies between Hamaker theory and molecular-simulation results have been found for thin films of LJ liquids[21] and SPC water[24] confined between two solid surfaces. In view of such results for liquids between confining solid surfaces where Lifshitz theory breaks down for very thin films, our MD results for free thin films are not unexpected. We again mention that it may be possible to redefine the film thickness to obtain a closer match to the theory, but such a definition is arbitrary.[25]

Actual thin-film force measurements employ surfactants and electrolytes in water, and the pressure in the vapor space is controlled by an inert gas such as air or nitrogen.[51] Consequently, we consider below the role of the inerts (that are used to control the pressure in the gas phase, p_N).

Water/Inert Gas Two-Component Films

Thermodynamics. For the one-component fluid discussed so far, there are 2 degrees of freedom of the thermodynamic system (i.e., that consisting of the thin film and the homogeneous-liquid reservoir). The additional degree of freedom compared to bulk phase equilibria is due to the curvature of the meniscus. Upon fixing the temperature, the remaining independent variable is the chemical potential (or alternately, film thickness or meniscus curvature). A constant-chemical-potential (or equivalently for a one-component fluid, a constant-pressure) reservoir, to reflect actual experimental measurement conditions, is not possible in a one-component system. Changes in the film thickness while maintaining the chemical potential of the liquid constant require that an inert gas be present in the thin-film apparatus. Accordingly, we introduce a similar component exhibiting a critical point well below the simulation temperature (to be called an inert gas from this point onward). In our simulations, the inert gas interacts with itself through a LJ potential with the parameters of $\sigma = 0.3681$ nm and $\epsilon = 763.73$ J/mol. The mass of the inert species is taken as that of nitrogen. Interaction between a water molecule and an inert molecule is also LJ, with the potential parameters determined by the Lorenz−Berthelot combining rule between σ and ϵ of the inert and the oxygen in water (i.e., $\sigma_{ij} = (\sigma_{ii} + \sigma_{jj})/2$ and $\epsilon_{ij} = (\epsilon_{ii}\epsilon_{jj})^{1/2}$). Thus, our initial simulation box consists of a liquid-film part containing water molecules and a gas part containing inert molecules. We allow the system to equilibrate for about 100 ps, whereby both components distribute between the film and gas phase, before averaging for about 200 ps.

Again, the disjoining pressure is defined by eq 2. Here, we first establish the properties of a thick film (corresponding to bulk coexistence for the two-component two-phase system) with a fixed number of inerts (i.e., setting the number of inert molecules in the gas phase is equivalent to imposing a given gas pressure). We then calculate the chemical potential of water and the normal pressure in our simulation box by the methods described above. This establishes the particular chemical potential of the water in the meniscus reservoir that is then kept constant for each different thin film. With a liquid meniscus of constant water chemical potential, the pressure in that meniscus changes as the film is thinned or thickened. The variation in pressure of the liquid meniscus is evaluated by integrating the Gibbs−Duhem equation, at fixed temperature and water chemical potential, between the chemical potential of inert gas in the thick and each thin film. In other words, the change in the meniscus liquid pressure is given by

$$p_{L,thin} - p_{L,thick} = \int_{\mu_{I,thick}}^{\mu_{I,thin}} \rho_I \, d\mu_I \qquad \text{at constant } T \text{ and } \mu_w \quad (7)$$

where the subscripts thick and thin refer to conditions of the liquid reservoir in equilibrium with the thick and the thin film, respectively, ρ_I is the density of the inert species solubilized in the bulk liquid phase, and μ_I is the corresponding chemical potential of the inert gas. Π for a particular thin film is then given by the difference between the spatially constant normal pressure calculated in the vapor region of that film and $p_{L,thin}$ for that thin film calculated from eq 7.

Unlike the case of pure water films where we assumed that ρ_w in the liquid meniscus is approximately a constant (see eq 3), we cannot assume that ρ_I (or, equivalently, the solubility of the inert component) is constant in the liquid meniscus. Thus, we must use the exact relation between μ_I and ρ_I to evaluate the integral in eq 7, or

$$\beta\mu_I = \ln\rho_I - \ln\langle\exp(-\beta\Delta U_I)\rangle \quad (8)$$

where β is $1/kT$, and ΔU_I is the change in potential energy of a homogeneous system, characterized by N_w, N_I, V, and T, upon addition of one inert molecule. If the solubility of inert molecules in water is small ($\rho_I \ll \rho_w$), the added test inert molecule interacts only with water molecules, and ΔU_I is a function of ρ_w only (i.e., the dissolved gas is in Henry's region). Moreover, if the density of water in the meniscus is approximately a constant between the limits of integration, the second term on the right of eq 8 is also approximately a constant. These two assumptions allow the integral in eq 7 to be performed analytically to establish $p_{L,thin}$. We justify these assumptions later and also estimate an upper bound on the magnitude of the integral in eq 7. Here we mention that the upper bound on the difference between $p_{L,thin}$ and $p_{L,thick}$ is small compared to the difference between p_N for a thin film and $p_{L,thick}$ (equal to the normal pressure in the thick film) calculated explicitly in our simulations ($\Pi = p_N - p_{L,thin}$). In other words, the liquid pressure in the meniscus reservoir is approximately a constant between various thin films. Accordingly, for all practical purposes, Π in our simulations can be approximated by the difference between the normal pressure in the thin film and the normal pressure in the thick film, although we do include the correction given by eq 7 (as estimated by the two assumptions mentioned below eq 8) in the results reported later.

Simulation Details

We simulate the reference thick film by constructing a slab of 534 water molecules in the center of the simulation box surrounded by 300 inert gas molecules. The schematic of the simulation system is, again, represented by Figure 1 with the inert gas now also present in the simulation box. L_x ($=L_y$) for this thick film is 2 nm. L_z is, again, 10 nm and remains constant for each thin film. The number of inert molecules chosen in the thick-film calculation is arbitrary. In our simulation, the number of inert molecules for the thick film corresponds to a pressure about 2 orders of magnitude larger than the vapor pressure of water at the simulation temperature (1.8 MPa at 479 K). The reason for choosing such a high pressure is to provide statistically significant differences in the pressures needed in the calculation of Π (see eq 2).

After simulating the thick film, we consider a thin-film system, iterating with different numbers of inert molecules until

TABLE 2: Simulated Quantities of Water/Inert-Gas Films at 479 K[a]

Film	$L_x(=L_y)$ (nm)	N_I	$\rho_{v,w}$ (g/cm^3)	$\rho_{v,I}$ (g/cm^3)	μ_w*	μ_I*	p_N (MPa)	Π (MPa)	h (nm)
6	2.00	300	0.0107	0.604	−23.7(3)	11.4	268.6	0	4.35
7	3.02	875	0.0113	0.556	−23.8(5)	8.0	241.1	−26.2	1.96
8	3.16	875	0.0198	0.496	−23.5(5)	4.8	195.2	−71.2	1.58
9	3.27	850	0.0217	0.447	−23.5(5)	2.1	157.4	−108.5	1.45
10	3.44	850	0.0283	0.387	−24.0(5)	−0.22	126.5	−139.2	1.22

[a] Film 6 represents a thick film ($\Pi = 0$).

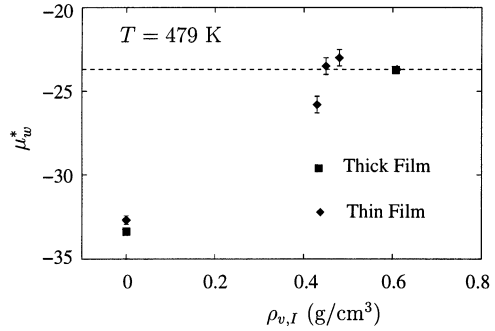

Figure 4. Chemical potential of water as a function of the gas-phase density of inert molecules in the simulation box, for both the thick and a thin film. The chemical potential obtained for the thick film is shown as a dashed line. Here the thin film in equilibrium with the homogeneous liquid meniscus has an inert gas density of 0.45 g/cm^3 corresponding to Film 9 in Table 2.

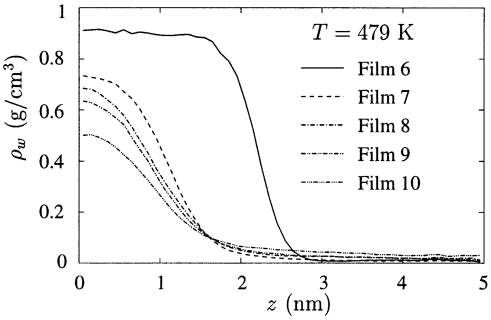

Figure 5. Water density profiles for five different water/inert-gas films at 479 K. Film 6 is a thick film ($\Pi = 0$), and Films 7−10 are progressively thinner.

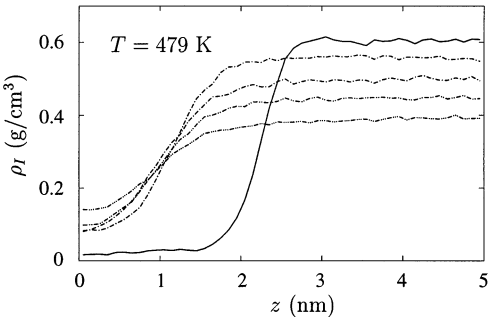

Figure 6. Inert-gas density profiles for five different water/inert-gas films at 479 K. The line notation is the same as in Figure 5.

the calculated chemical potential of water in the thin film equals the value calculated for the reference thick film. Figure 4 depicts this trial-and-error procedure for one particular thin film (with $L_x = L_y = 3.27$ nm) by plotting the calculated chemical potential of water (μ_w*) against the simulated density of inert molecules in the gas phase, $\rho_{v,I}$. [Although in the trial-and-error procedure the number of inert molecules (N_I) is varied directly, it is more informative to plot $\rho_{v,I}$ in Figure 4. This is to make it clear that even though N_I increases from the thick to the thin film (from 300 in the thick film to 850 in the thin film at the same water chemical potential), $\rho_{v,I}$ decreases, explaining the trend toward the decrease in p_N from the thick to the thin film seen in Table 2 later.] Closed squares represent the chemical potential of water in the thick films, whereas diamonds represent the chemical potential of water in thin films with different $\rho_{v,I}$ calculated from our simulations. The corresponding symbols at $\rho_{v,I}$ equal to zero correspond to pure water films for the same L_x and L_y without the inert present. A dashed line reflects the desired value of chemical potential obtained with the thick film. Hence, in Figure 4, the thin film with $\rho_{v,I} \approx 0.45$ g/cm^3 has the same value of water chemical potential as the thick film (with $\rho_{v,I} \approx 0.61$ g/cm^3).

Given the effort required for this trial-and-error procedure, it is desirable to fix externally the chemical potential of water for the thin films at the required value as in a grand-canonical ensemble. Unfortunately, for free thin films, Winter has demonstrated that the films evaporate/condense as soon as particle-exchange moves (as in the grand-canonical ensemble) with a reservoir are allowed.[43] A canonical ensemble appears necessary for an unstable thin film to remain intact.

Results. Table 2 lists the simulated properties of each film in contact with the inert gas. Column 2 shows L_x ($=L_y$), column 3 reports N_I, column 4 shows $\rho_{v,w}$, column 5 lists the inert density in the vapor phase above the film ($\rho_{v,I}$), column 6 gives μ_w* with the numbers in parentheses denoting the error in the last reported significant digit, column 7 highlights μ_I* (chemical potential of inert species relative to the density-independent part[45] and nondimensionalized with respect to ϵ_{oo}), and column 8 displays p_N for each film. Density profiles of water for each film are shown in Figure 5 while the density profiles for the inert gas in each film are depicted in Figure 6. Film 6 is a thick film, and the densities of the water and the inert molecules in both the liquid and gas regions, as shown by Figures 5 and 6, correspond to two-phase coexistence of this two-component system. For Films 7−10, the density of water at the center of the films is lower than the coexistence density, whereas the density of water in the gas phase over the thinner films is progressively larger (see Table 2). The inert-gas density profiles shown in Figure 6 display a trend toward smaller density of inert molecules in the vapor phase as the films are thinned (Films 6−10). Since the vapor region is dominated by the inert gas, the above observation indicates that the normal pressure decreases as the films are thinned, consistent with the negative values of Π. In the inhomogeneous liquid parts of Films 7−0, similar to water in Figure 5, the densities of inert molecules in Figure 6 do not reflect the densities of inert molecules in the corresponding homogeneous liquid reservoirs in equilibrium with these thin films (which values have not been calculated).

For each film, the disjoining pressure is calculated from eq 2 as discussed above. The results are shown in column 9 of Table 2. Before proceeding further, we refer back to the assumptions adopted in eq 8 and used to calculate Π. From Figures 5 and 6 we find that for the thick film (Film 6), the solubility of inert gas in the liquid part of the film is small, although not negligible ($\rho_{L,w} = 0.904$ g/cm^3, $\rho_{L,I} = 0.024$ g/cm^3, and the mole fraction of the inert gas in liquid water is 0.0167).

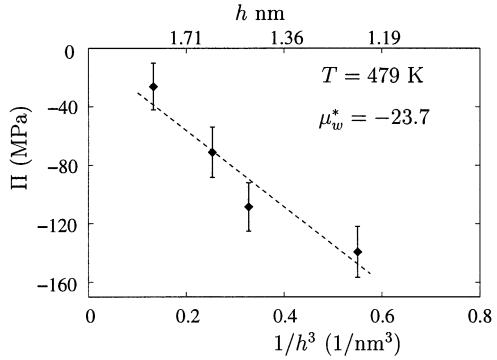

Figure 7. Disjoining-pressure isotherm for water/inert gas films at 479 K and $\mu_w^* = -23.7$ ($p_L = 266$ MPa). The dashed line represents a best fit to the data.

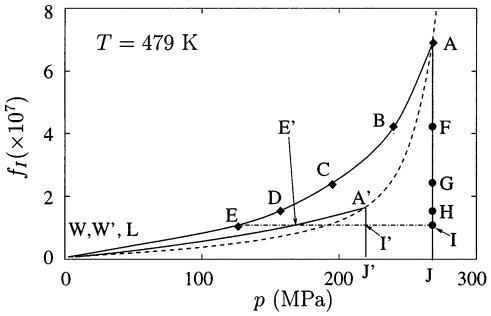

Figure 8. Plot of $f_I - p$ with μ_w as a parameter for the two-component system at 479 K. Points A−E represent Films 6−10, respectively. The line A to W corresponds to $\mu_w^* = -23.7$. A description of the remaining lines is given in the text.

Since Film 6 is a thick film, the solubility of the inert gas in the corresponding homogeneous liquid reservoir is the same as that in the homogeneous liquid portion of the film. Now for thinner Films 7−10, column 7 of Table 2 shows that the chemical potential of the inert gas in the homogeneous liquid reservoir in equilibrium with these films is progressively smaller than the corresponding value for the thick film. Thus, the density of the inert gas in the meniscus in equilibrium with these thin films must be smaller than that for the reservoir in equilibrium with the thick film. Here, we again note that the density of the inert gas in the center of the thin films is not the same as the density of the inert in the corresponding liquid reservoir.

Due to the low solubility of the inert gas, we can now justify the approximations of Henry's law and an incompressible liquid reservoir made in calculating Π. For example, $p_{L,thin} - p_{L,thick}$ obtained for Film 10 with the assumptions outlined below eq 8 equals −2.9 MPa. This number is, then, added to the difference between p_N of Film 10 and Film 6 to obtain the value of Π given in column 9 for Film 10. An upper bound estimate of $p_{L,thin} - p_{L,thick}$ proceeds as follows. Since $\rho_{L,I}$ is maximum for the reservoir in equilibrium with the thick film (Film 6), the upper bound on the integral in eq 7 is simply this value of $\rho_{L,I}$ multiplied by the difference of μ_I between the thick and the thin films. Again for Film 10, this value is −6.4 MPa. When compared with the more refined −2.9-MPa estimate in the context of the 142.1-MPa difference between the normal pressures of Films 6 and 10, we note that the correction to Π from eq 7 is small (although we use the refined estimate in reporting column 9 of Table 2). Hence, even though it is possible to simulate separately the homogeneous liquid-reservoir conditions to obtain $p_N - p_{L,thin}$ directly (e.g., using a grand-canonical ensemble to get the reservoir conditions at the desired chemical potentials of water and the inert gas), such a calculation adds only a minor correction to our results.

The film thickness for each thin film is calculated by assuming a step-function density profile between the liquid and the vapor region and by imposing zero adsorption of water at the dividing surface as noted previously for pure water and LJ[25] films. In the usual definition of the film thickness, however, $\rho_{L,w}$ is the density of water in the homogeneous liquid in equilibrium with the thin film. We do not have this value from our simulations; hence we adopt $\rho_{L,w}$ obtained for the thick film. However, as in the case of water-only films, we expect the meniscus−water density for each thin film to be almost the same as that for a thick film. Film thickness, *h*, is tabulated in column 10 of Table 2; Figure 7 shows Π as a function of $1/h^3$ for the thin films surrounded by inert gas. The points represent the MD result for the two-component system. Errors in Π are estimated from the corresponding errors in evaluating μ_w. In addition, the dashed line shows the best-fit straight line to the MD results. Upon comparing the MD results for the one-component to the two-component system, we notice that the magnitudes of Π and the apparent Hamaker constant are about twice as large as those for pure water films for the conditions simulated.

Role of Inert Gas

We now address the issue of the effect of changing the gas pressure (or, equivalently, the number of inert molecules) applied to the reference thick film on Π to understand how the results are affected if simulations are performed at lower, and more realistic, pressures. Figure 8 graphs the isothermal absolute activity of the inert gas, $f_I = \exp(\beta\mu_I)$, as a function of pressure with μ_w as a parameter. Values of f_I and p_N for Films 6−10, which have the same μ_w, are shown in this diagram as closed diamonds A to E, respectively. The solid line passing through points A to E is a schematic of the loci of the continuum of films with properties between Films 6 to 10 and beyond. It is possible that at $\mu_w^* = -23.7$ (the value for these films), pure water vapor may not exist when $f_I = 0$. Hence, the extension of this solid line to $f_I = 0$ at point W is not quantitative. We outline the behavior of this extension near $f_I = 0$ in Appendix B. Closed circles F−I in Figure 8 depict f_I and p_L of the homogeneous meniscus reservoirs (at $\mu_w^* = -23.7$) in equilibrium with Films B−E, respectively. The solid, almost vertical, line AJ is a locus of the conditions in the meniscus reservoirs, analogous to the solid line through points A−E and beyond. This line is calculated from eqs 7 and 8. The fact that line AI is almost vertical reiterates our comments above that keeping μ_w constant in the simulations is essentially equivalent to maintaining a constant pressure in the liquid meniscus reservoir. The magnitude of Π for each thin film is given by the horizontal distance between the closed diamonds and closed circles. For example, the distance between points E and I is depicted by the dashed−dotted line. The distance along the ordinate between point W (when it exists) and point J gives the disjoining pressure for the terminal, zero-inert-gas pure water thin film. As the gas-phase pressure is raised over the films (W, E, D, etc.) the magnitude of disjoining pressure falls in line with the more dense and, hence, thicker films (see Figures 5 and 6).

The results presented in Table 2 and Figure 7 correspond to about 2 orders of magnitude larger pressure (i.e., ca. 250 MPa) than the vapor pressure of water at 479 K (i.e., 1.8 MPa). Experimental measurement of disjoining pressures are conducted at much lower pressures. The effect of changing the gas pressure imposed on films can be qualitatively deduced from Figure 8. First, we note that point A (for Film 6) corresponds to a thick film, and thus, lies on the two-component water/inert-gas bulk coexistence curve. Other points along this bulk-coexistence

curve are indicated schematically by the dashed line A′L in Figure 8. All thick films at lower pressures must fall along this dashed line with f_l lower than f_l at point A. To illustrate, we choose schematically a reference thick film with a lower pressure (point A′) lying on the dashed two-phase coexistence curve. As mentioned above, the chemical potential of water at point A′ is different from that at point A. As with point A, point A′ generates a set of thin films with a new constant μ_w equal to that at point A′. This second collection of lower pressure thin films is depicted schematically by the solid curve passing through A′E′ and terminating at point W′ at $f_l = 0$. Line A′I′J′ represents the conditions of the corresponding lower pressure homogeneous liquid meniscus reservoir at $\mu_{w,A'}$ in equilibrium with the films at different f_l values. Π for a particular film at lower pressure, say that at E′, is given by the pressure difference between points E′ and I′.

Clearly from Figure 8, as the pressure over the collection of reference thick film decreases (i.e., along the dashed line), Π for a given f_l decreases (i.e., compare the distances EI and E′I′). Thus, as we increase the gas-phase pressure along the lower pressure thin-film collection, W′E′A′, the films thicken because of increased film densities, and the disjoining pressure diminishes along the collection of thin films W′E′A′. Now, however, the overall gas pressures are lower and the disjoining pressures are smaller. Consequently, the role of increasing the inert gas pressure over a thin water film is to thicken it, thereby decreasing the magnitude of the attractive thin-film forces. The lower the absolute gas pressure is, the smaller is the effect.

Conclusions

In this work, we extend our previous work for LJ systems to calculate disjoining-pressure isotherms for aqueous systems. First, we consider pure water (one component) films at 479 K using the SPC/E intermolecular potential model. Due to the negligible number of molecules in the vapor phase and the corresponding lack of statistical significance, we cannot calculate $\Pi(h)$ at ambient temperatures. At 479 K, we find results qualitatively similar to those for the LJ films of our previous work. In particular, the chemical potential of water increases as the films thin. Also, the density of water at the center of thin films falls below the bulk coexistence density. Calculated disjoining-pressure isotherms for these water films, when compared to the standard Lifshitz theory, indicate that the disjoining pressures for water are about 2 orders of magnitude larger for films between about 1 to 2 nm thickness. This is most likely, in view of our previous work, due to the fact that the standard theory assumes that fluid properties are homogeneous directly up to the interface and neglects any fluid structure.

We then added an inert-gas component because in actual thin-film force experiments the pressure of the gas phase is controlled by an inert component (i.e., air). This extension allows us to keep the chemical potential of water in the reservoir as a constant for films of various thicknesses, and requires reformulation of the calculation of the disjoining pressure. For a high-pressure, two-component system the disjoining pressures calculated by MD are about twice as large as those calculated for pure water films. From qualitative arguments we find that upon decreasing the reference pressure, and, thereby, decreasing the chemical potential of water, a different set of thin films with correspondingly smaller disjoining pressures is obtained.

Appendix A: Ewald Parameters

Ewald summation for the coloumbic part of the intermolecular potential and for the LJ part has been discussed in great detail in the literature.[36,37] Here, we briefly mention that the Ewald-summation method divides the intermolecular potential sum into a real-space part and a Fourier-space part and requires a real-space cutoff (r_{cut}), a real-space convergence parameter (α), and a maximum number of wave vectors ($|\mathbf{h}_{max}|$) considered in the Fourier-space sum to be specified. Given r_{cut}, the remaining parameters can be determined by accuracy requirements, as has been shown in detail by Karasawa and Goddard.[37] In our simulations, $r_{cut} = 0.98$ nm, and we follow Goddard and Karasawa to determine α and $|\mathbf{h}_{max}|$ by specifying that the error due to cutoff in the Ewald method is an order of magnitude smaller than that without the Ewald method but with the same cutoff.

Additionally, since our simulation box is not cubic, we must allow for a different number of wave vectors in each direction.[35] Now, **h** is given by

$$\mathbf{h} = \frac{2\pi}{L_x} n_x \mathbf{i} + \frac{2\pi}{L_y} n_y \mathbf{j} + \frac{2\pi}{L_z} n_z \mathbf{k} \qquad \text{(A1)}$$

where n_x, n_y, and n_z are the number of wave vectors in the x, y, and z directions, respectively, and **i**, **j**, and **k** are the unit vectors. In our simulations, we keep the density of wave vectors a constant in each direction. Specifically, since $L_x = L_y \neq L_z$, we keep the ratio of wave vector the same as the ratio of nearest integer of the box lengths in the three directions.

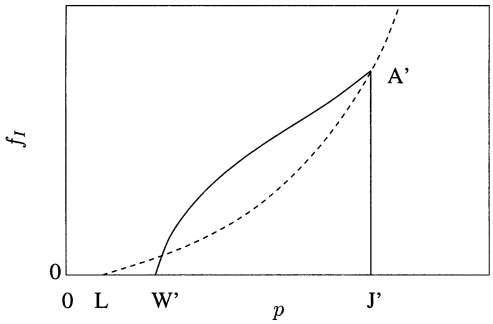

Figure 9. Schematic of f_l−p plot of Figure 8 with emphasis on the region near $f_l = 0$. Point L represents the bulk coexistence for pure water. More details are given in Appendix B.

Appendix B: Near $f_l = 0$

Here, we discuss the scenario near $f_l = 0$ in Figure 8. Even though the solid line through points A−E may not exist down to $f_l = 0$, there are some sets of constant μ_w thin films with a lower value of μ_w that do extend to $f_l = 0$. In other words, μ_w for one of these sets lies below the vapor spinodal for pure water at $\mu_{w,s}$. For this case, we show schematically in Figure 9 the region of Figure 8 near $f_l = 0$. The solid line A′W′ represents the conditions of thin films with $\mu_w < \mu_{w,s}$. Point A′ is the bulk coexistence point for a particular $f_l \neq 0$. Accordingly, the dashed line A′L represents the bulk two-phase coexistence curve for the two-component system. The pressure at point L (pure-water coexistence) is lower than the normal pressure at point W′ because the pressure in the metastable pure-water vapor is higher than that at pure-water coexistence. Lines A′W′ and A′L do not actually intersect because μ_w is not the same for both at the projected apparent intersection point in Figure 9. The solid line A′J′ represents the conditions of the homogeneous meniscus reservoirs in equilibrium with the thin films between points A′ and W′. As before, the magnitude of Π at a particular f_l is given by the horizontal distance between lines A′W′ and A′J′ at that f_l. For the set of films between points A′ and W′, as the number of inert molecules decreases to zero ($f_l = 0$), the magnitude of

Π is the difference in pressure between points W′ and J′. Hence, for the particular film at W′ (out of the set A′W′), the value of Π is the same as that for a pure-water film at the same μ_w*. For example, if μ_w for this set of thin films is -31.9, Π for the film at W′ is the same as that for pure-water film 4 (cf. Table 1).

Thus, for a set of films with $\mu_w < \mu_{w,s}$, the value of Π for the thinnest film (the extreme case film with $f_l = 0$) must coincide with one particular pure-water film with the same μ_w. For the rest of the thin films with inert gas from that particular set (i.e., with the same μ_w but a higher pressure), the magnitude of Π is smaller. However, these values of Π from the two-component set A′W′ cannot be compared meaningfully with those of the rest of the pure-water films (apart from that particular film with the same μ_w). For example, if μ_w* is -31.9 for the set A′W′, the values of Π for the films in the two-component set can be either larger or smaller (depending on the pressure of the reference thick film A′) than those of the rest of pure-water films (apart from film 4, as mentioned above, and film 5, because the magnitude of Π for film 5 is larger than that for film 4).

With the preceding discussion, it is clear that even in the limit of a very small number of inert molecules in the reference thick film, the disjoining-pressure isotherms for a two-component system and the pure-water system cannot coincide. The reason is that in the limit of very small number of inert molecules in the reference thick film, μ_w for different thin films is kept at a constant value. This can be contrasted with pure water films for which μ_w must be changed for different thin films due to the lack of sufficient degrees of freedom. The disjoining-pressure isotherms for the two-component and the pure-water systems would coincide in the limit of no inert molecules only if we redefined the calculation of disjoining pressure for two-component systems by keeping μ_l constant for a set of films (e.g., films 6−10, hypothetically) and varied μ_w to access these different films. However, this redefinition of the calculation is not consistent with those actual experiments in which the pressure of the gas phase is varied across different film thicknesses.

In contrast, for actual experiments in which the pressure of the gas phase is kept constant and different film thicknesses are obtained by varying the pressure of the homogeneous liquid reservoir, the situation is perhaps closer to keeping μ_l constant and varying μ_w for a particular set of films because the gas phase is dominated by the inert gas. For such experiments, the disjoining-pressure isotherm for the particular set in the limit of very few inert molecules approaches the disjoining-pressure isotherm for pure-water films, as mentioned above.

References and Notes

(1) Davis, H. T.; Scriven, L. E. *Adv. Chem. Phys.* **1982**, *49*.
(2) Derjaguin, B. V.; Churaev, N. V. *Kolloidn. Zh.* **1976**, *38*, 402.
(3) Derjaguin, B. V.; Churaev, N. V. *J. Colloid Interface Sci.* **1978**, *66*, 389.
(4) Kruglyakov, P. M. *Thin Liquid Films*; Ivanov, I. B., Ed.; Marcel Dekker: New York, 1988; Chapter 11.
(5) Ivanov, I. B. *Colloids Surf. A* **1997**, *128*, 155.
(6) Mysels, K. J.; Jones, M. N. *Discuss. Faraday Soc.* **1966**, *42*, 42.
(7) Exerowa, D.; Kolarov, T.; Khristov, K. H. R. *Colloids Surf.* **1989**, *22*, 171.
(8) Kolarov, T.; Cohen, R.; Exerowa, D. *Colloids Surf.* **1989**, *42*, 49.
(9) Bergeron, V.; Radke, C. J. *Langmuir* **1992**, *8*, 3020.
(10) Bergeron, V.; Radke, C. J. *Colloid Polym. Sci.* **1995**, *273*, 165.
(11) Karraker, K. A.; Radke, C. J. *Adv. Colloid Interface Sci.* **2002**, *96*, 231.
(12) Exerova D.; Zacharieva, M. *Research in Surface Forces*; Derjaguin, B. V., Ed.; Consultants Bureau: New York, 1972; Vol. 4, p 253.
(13) Bergeron, V.; Waltermo, A.; Claesson, P. M. *Langmuir* **1996**, *12*, 1336.
(14) Sedev, R.; Nemeth, Z.; Ivanova, R.; Exerowa, D. *Colloids Surf. A* **1999**, *149*, 141.
(15) Cascao Pereira, L. G.; Johansson, C.; Blanch, H. W.; Radke, C. J. *Colloids Surf. A* **2001**, *186*, 103.
(16) Bergeron, V.; Langevin, D.; Asnacios, A. *Langmuir* **1996**, *12*, 1550.
(17) Gallego, L. J.; Rey, C.; Grimson, M. J. *Mol. Phys.* **1991**, *74*, 383.
(18) Magda, J. J.; Tirrel, M.; Davis, H. T. *J. Chem. Phys.* **1985**, *83*, 1888.
(19) Dickman, R.; Anderson, P. E. *J. Chem. Phys.* **1993**, *99*, 3112.
(20) Jimenez, J.; Rajagopalan, R. *Eur. Phys. J. B* **1998**, *5*, 237.
(21) Berard, D. R.; Attard, P.; Patey, G. N. *J. Chem. Phys.* **1993**, *98*, 7236.
(22) Luzar, A.; Bratko, D.; Blum, L. *J. Chem. Phys.* **1987**, *86*, 2955.
(23) Shinto, H.; Miyahara, M.; Higashitani, K. *J. Colloid Interface Sci.* **1999**, *209*, 79.
(24) Forsman, J.; Jonsson, B.; Woodward, C. E. *J. Phys. Chem.* **1996**, *100*, 15005.
(25) Bhatt, D.; Newman, J.; Radke, C. J. *J. Phys. Chem. B* **2002**, *106*, 6529.
(26) Chambers, K. T.; Radke, C. J. *Interfacial Phenomena in Petroleum Recovery*; Morrow, N. R., Ed.; Marcel Dekker: New York, 1990; p 211.
(27) Weng, J.-G.; Park, S.; Lukes, J. R.; Tien, C.-L. *J. Chem. Phys.* **2000**, *113*, 5917.
(28) Hamaker, H. C. *Physica IV* **1937**, *10*, 1058.
(29) Ninham, B. W.; Parsegian, V. A.; Weiss, G. H. *J. Stat. Phys.* **1970**, *2*, 323.
(30) Berendsen, H. J. C.; Grigera, J. R.; Straatsma, T. P. *J. Phys. Chem.* **1987**, *91*, 6269.
(31) Nose, S. *Mol. Phys.* **1984**, *52*, 255.
(32) Hoover, W. G. *Phys. Rev. A* **1985**, *31*, 1695.
(33) Frenkel, D.; Smit, B. *Understanding Molecular Simulations*; Academic Press: New York, 1991; Chapter 6.
(34) Allen, M. P.; Tildesley, D. J. *Computer Simulation of Liquids*; Clarendon Press: Oxford, UK, 1987; Chapter 7.
(35) Alejandre, J.; Tildesley, D. J.; Chapela, G. A. *J. Chem. Phys.* **1995**, *102*, 4574.
(36) de Leeuw, S. W.; Perram, J. W.; Smith, E. R. *Proc. R. Soc. London, Ser. A* **1980**, *373*, 27.
(37) Karasawa, N.; Goddard, W. A. *J. Phys. Chem.* **1989**, *93*, 7320.
(38) Wheeler, D. R.; Rowley, R. L. *Mol. Phys.* **1998**, *94*, 555.
(39) Irving, J. H.; Kirkwood, J. G. *J. Chem. Phys.* **1950**, *18*, 817.
(40) Walton, J. P. R. B.; Tildesley, D. J.; Rowlinson, J. S. *Mol. Phys.* **1983**, *48*, 1357.
(41) Nose, S.; Klein, M. L. *Mol. Phys.* **1983**, *50*, 1055.
(42) Widom, B. *J. Statistical Phys.* **1978**, *19*, 563.
(43) Winter, S. J. Ph.D. Dissertation, University of California, Berkeley, 1999, Chapter 3.
(44) Huang, D. M.; Geissler, P. L.; Chandler, D. *J. Phys. Chem. B* **2001**, *105*, 6704.
(45) Hill, T. L. *An Introduction to Statistical Thermodynamics*; Dover Publications: New York, 1986; Chapters 4 and 8.
(46) de Feijter, J. A. *Thin Liquid Films*; Ivanov, I. B., Ed.; Marcel Dekker: New York, 1988; Chapter 1.
(47) Overbeek, J. Th. G. *Colloid Science I*; Kruyt, H. R., Ed.; Elsevier: Amsterdam, The Netherlands, 1952; Chapter 6.
(48) Lifshitz, E. M. *Sov. Phys. JETP* **1956**, *2*, 73.
(49) Dagastine, R. R.; Prieve, D. C.; White, L. R. *J. Colloid Interface Sci.* **2000**, *231*, 351.
(50) Israelachvili, J. N. *Intermolecular and Surface Forces*; Academic Press: New York, 1991; Chapter 13.
(51) Claesson, P. M.; Ederth, T.; Bergeron, V.; Rutland, M. W. *Adv. Colloid Interface Sci.* **1996**, *67*, 119.